UCRL-JC-132585
Preprint

Electron Heat Transport in Improved Confinement Discharges in DIII-D

B.W. Stallard, C.M. Greenfield, G.M. Staebler, C.L. Rettig, M.S. Chu, M.E. Austin, D.R. Baker, L.R. Baylor, K.H. Burrell, J.C. DeBoo, J.S. deGrassie, E.J. Doyle, J.Lohr, G.R. McKee, R.L. Miller, W.A. Peebles, C.C. Petty, R.I. Pinsker, B.W. Rice, T.L. Rhodes, R.E. Waltz, L. Zeng, and the DIII-D Team

This paper was prepared for submittal to

40th Annual Meeting, APS Division of Plasma Physics
New Orleans, LA
November 16-20, 1998

November 24, 1998

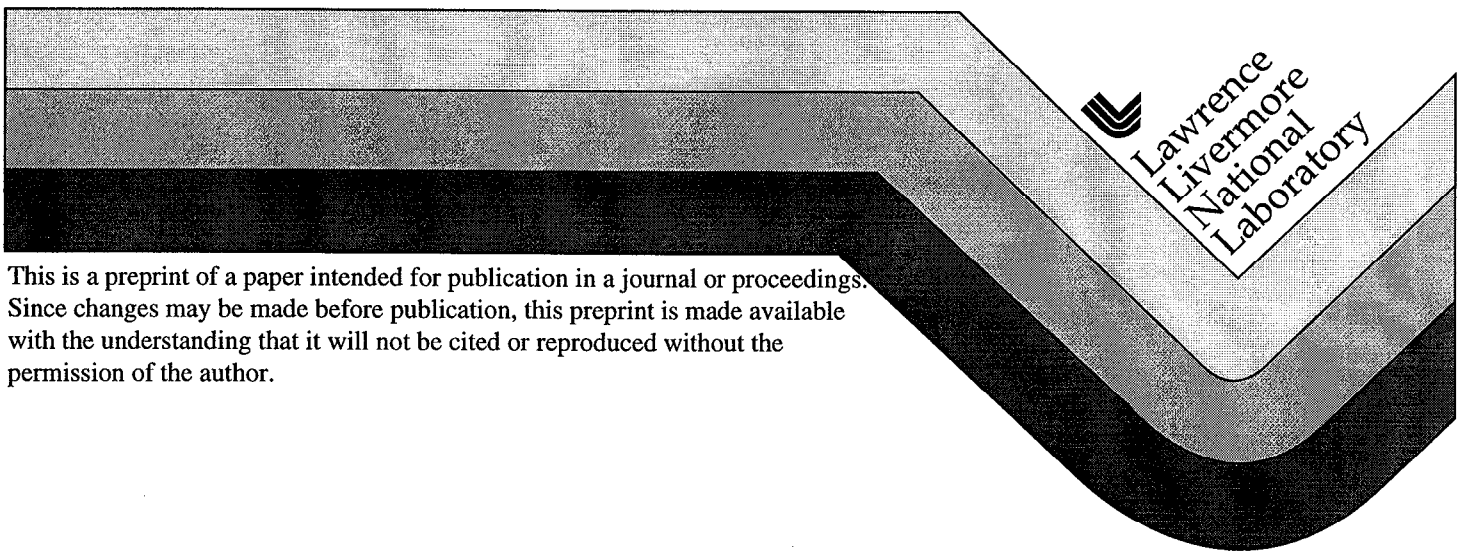

Electron heat transport in improved confinement discharges in DIII-D

B.W. Stallard,[a] C.M. Greenfield,[b] G.M.Staebler,[b] C.L. Rettig,[c] M.S. Chu,[b] M.E. Austin,[d] D.R. Baker,[b] L.R. Baylor,[a] K.H. Burrell,[b] J.C. DeBoo,[b] J.S. deGrassie,[b] E.J. Doyle,[c] J. Lohr,[b] G.R. McKee,[e] R.L.Miller,[b] W.A. Peebles,[c] C.C. Petty,[b] R.I. Pinsker,[b] B.W. Rice,[a] T.L.Rhodes,[c] R.E. Waltz,[b] L. Zeng,[c] and THE DIII–D TEAM

[a]Lawrence Livermore National Laboratory, Livermore, California.
[b]General Atomics, P.O. Box 85608, San Diego, CA 92186-5608
[c]University of California, Los Angeles, California.
[d]University of Texas at Austin, Austin, Texas.
[e]University of Wisconsin, Madison, Wisconsin.

(Received

Abstract

In DIII–D tokamak plasmas with an internal transport barrier (ITB), the comparison of gyrokinetic linear stability (GKS) predictions with experiments in both low and strong negative magnetic shear plasmas provide improved understanding for ion and electron thermal transport within much of the plasma. As previously reported, the region for improved ion transport seems well characterized by the condition $\omega_{ExB}>\gamma_{max}$, where ω_{ExB} is the *ExB* flow shear, calculated from measured quantities, and γ_{max} is the maximum linear growth rate for ion temperature gradient (ITG) modes in the absence of flow shear. Within a limited region just inside the ITB, the electron temperature gradient (ETG) modes appear to control the electron temperature gradient and, consequently, the electron thermal transport. The increase in electron temperature gradient with more strongly negative magnetic shear is consistent with the increase in the ETG mode marginal gradient. Closer to the magnetic axis the T_e profile flattens and the ETG modes are predicted to be stable. With additional core electron heating, FIR scattering measurements near the axis show the presence of high k fluctuations (12 cm^{-1}), rotating in the electron diamagnetic drift direction. This turbulence could impact electron transport and possibly also ion transport. Thermal diffusivities for electrons, and to a lesser degree ions, increase. The ETG mode can exist at this wavenumber, but it is computed to be robustly stable near the axis. Consequently, in the

plasmas we have examined, calculations of drift wave linear stability do not explain the observed transport near the axis in plasmas with or without additional electron heating, and there are likely other processes controlling transport in this region.

I. INTRODUCTION

Tokamak plasma discharges with advanced performance, as measured by normalized plasma pressure (β_N) and energy confinement factor (H), have been routinely achieved in numerous large machines (e.g., DIII–D,[1] TFTR,[2] JET,[3] JT60-U[4]) in recent years. Many of these experiments employ early heating during the current ramp up (e.g. neutral beam injection) to create a current profile with negative central magnetic shear (NCS) within the core of the plasma and with safety factor q>1. When sufficient heating power is applied, these conditions are conducive to creation of an internal transport barrier (ITB). Here, magnetic shear is defined by $s= r/q\ (dq/dr)$. Following the current ramp, an increase of neutral beam power expands the transport barrier in a high performance phase. During this time, reduction of the ion thermal diffusivity to the neoclassical level within the ITB has been observed.[1] The region for reduced ion transport is well characterized by the condition $\omega_{ExB}>\gamma_{max}$, where ω_{ExB} is the rate of*ExB* flow shear,[5] determined from measured quantities, and γ_{max} is the theoretical maximum linear growth rate for ion temperature gradient (ITG) modes in the absence of flow shear.[6] Consistent with the observed reductions in ion heat diffusivity, low-k turbulence ($k < 2$ cm^{-1}), measured by beam emission spectroscopy and far infrared scattering (FIR), also decreases within the same region.[7]

In DIII–D ITB plasmas, large reductions in transport are observed in the ion (χ_i), angular momentum (χ_ϕ), and sometimes particle (D) diffusivities, but a similar large reduction in electron heat transport (χ_e) is often not observed. In low magnetic shear plasmas, χ_e shows little change, and remains well above χ_i. However, in some DIII–D discharges with strongly negative magnetic shear, larger reductions in χ_e have been observed; our results are similar to those reported from other tokamaks.[8,9] The electron temperature profile steepens just inside the ion ITB, indicating formation of an electron ITB. In this region χ_e may decrease a factor 3–10, but remains far above the neoclassical level. Closer to the magnetic axis, χ_e then increases again.

In this paper, we restrict our discussion to plasmas with an ITB and an L–mode edge. A central focus of the work is to test the hypothesis[10] that electron temperature gradient (ETG) modes control the electron thermal transport. We compare transport determined by power balance analysis with the predictions of drift wave linear stability theory, including the short wavelength (high k) ETG modes.[11] The instability which causes the electron thermal transport must be able to exist in a large *ExB* shear

environment and must primarily affect electron transport, but have little effect on the ions, consistent with observations that $\chi_i << \chi_e$ in these discharges. The ETG mode has a large poloidal wave number (k) and a large growth rate $\gamma > \omega_{ExB}$. Due to finite Larmor radius effects, the ETG mode is expected to produce little ion transport.

In Section II, we compare experimental transport against the predictions of linear drift wave theory for both low and strong NCS discharges, heated by neutral beams. Several conclusions result from this work. Just inside the ITB, where χ_i falls and the condition $\omega_{ExB} \geq \gamma_{max}$ is satisfied for ITG modes, the experimental electron gradient, ∇T_e, increases as the predicted critical gradient, $\nabla T_{e_{crit}}$ for the ETG mode increases. This result holds in both low magnetic shear and strong *negative* magnetic shear, and provides strong support for the hypothesis that the ETG mode controls transport within this region. Closer to the magnetic axis, the electron temperature profile flattens, and ETG modes are predicted stable. However, χ_e is still large there; consequently linear drift wave theory does not explain transport for the electrons in this region. Some other process(es) must control electron thermal transport there. In Section III, we present results where electron heating is added to beam heated discharges with an ITB and discuss our measurements of high k fluctuations near the magnetic axis. In that region, while fluctuations at *high-k* are observed to increase with electron heating, linear drift wave theory does not explain the observed transport since it again predicts all modes are stable. Discussions and a summary follow in Section IV.

II. TRANSPORT AND THEORY IN BEAM HEATED PLASMAS

A. Transport and data analysis

We have used standard methods of power balance analysis to infer thermal diffusivities, using TRANSP[12] and measured profiles of temperatures, electron and carbon impurity densities, and radiated power. For this analysis, although heat flow is dominated by conduction, because of imprecise knowledge of particle sources and lack of on-axis density measurements, we define thermal diffusivities from the total power flow, i.e., $\chi_{i,e}^{tot} = -q_{tot_{i,e}} / (n_{i,e} \nabla T_{i,e})$ for the main ions and electrons.

To determine the *ExB* shearing rate to compare against turbulence growth rates, we calculate the electric field profile from force balance analysis, using the carbon impurity ion temperature and density and poloidal and toroidal rotation velocities, measured by charge exchange recombination.[13] The safety factor profile q was obtained from EFIT[14] equilibrium reconstruction, constrained by motional Stark effect measurements of the vertical magnetic field, corrected for the local radial electric field.[15]

B. Gyrokinetic drift wave calculations

A comprehensive gyrokinetic stability (GKS) code, was used to calculate linear growth rates for toroidal drift waves in the absence of *ExB* shear. The code treats electrons and two ion species (main ion and impurity). The original code[16] has been extended[17] to include noncircular geometry,[18] including both the full electromagnetic response and the Debye length shielding for electrons. The GKS code does not predict he experimental diffusivity, since the actual transport would result from the saturated levels (nonlinear) of turbulent modes in the presence of the flow shear.

C. Transport in low magnetic shear

Figure 1(a) shows the q profile and measured plasma temperatures at two times, t = 1.52 s, during low power (5.2 MW), and at t = 1.82, during high power (9.6 MW), following neutral beam power step-up at 1.6 s. Here $\rho = [\Phi/\Phi(a)]^{0.5}$, where a is the plasma radius and Φ is the toroidal flux. Transport barrier expansion and temperature increases are evident in the figure, but the electron temperature changes much less than the ion temperature. As shown in Fig. 1(b), the ion diffusivity decreases to the neoclassical level, but for the electrons within analysis uncertainties, there is no change in χ_e^{tot}.

In Fig. 2 we compare the experiment with the predictions of GKS modeling. For the low k ITG mode, Fig. 2(a) shows $\omega_{ExB} > \gamma_{max}$ for $\rho < 0.54$, indicating agreement between the region of calculated suppression of low k turbulence by *ExB* flow shear (shaded region in the figure) and the region with reduced transport for the ions. Figure 2(b) compares the results of GKS calculations for the high k ETG mode and the measured electron temperature behavior, characterized by the normalized electron temperature gradient $a/L_{T_e} = -(1/T_e)\, dT_e/d\rho$. The comparison between the experimental value and the calculated critical gradient for ETG instability $a/L_{T_e}^{crit}$, is shown in the figure, where the ETG mode is

unstable for $a/L_{T_e}^{\exp} > a/L_{T_e}^{crit}$. Outside $\rho = 0.54$, both ITG and ETG modes are predicted unstable, and, experimentally, both χ_e^{tot} and χ_i^{tot} are large.

Moving inside the ITB in the region $0.33 < \rho < 0.54$, $a/L_{T_e}^{\exp}$ follows an increasing value of $a/L_{T_e}^{crit}$, and the ETG mode is marginally stable. This result suggests that the ETG modes may be affecting the electron diffusivity within this region, although it should be noted that no fluctuation measurements at high k were made in this discharge to help support this suggestion. Within most of this region the magnetic shear is low and varies over the range $-0.16 < s < 0.6$. At smaller radius, the ETG is stable, but χ_e^{tot} does not decrease. This results suggests that some other process(es) controls transport near the axis.

Also shown in Fig. 2(b) is a region where $D_R > 0$, calculated by the BALOO code.[19] $D_R > 0$ is a necessary condition[20] indicating that resistive interchange activity may be present, driven by the local pressure gradient. The BALOO calculation is local and assumes very high mode number. It provides no information on the wavelength or frequency of unstable modes. During the higher performance period of many DIII–D L–mode NCS discharges, typically $D_R > 0$ and increases in time, sometimes preceding, and often following, small MHD bursts of low toroidal mode number (e.g., n=1 and localized to the q=2 or 3 surfaces). Local flattening of the T_e profile can be seen with second harmonic electron cyclotron emission for such events. MARS code[21] analysis of low n modes for these events has identified resistive interchange instability or resistive kink modes, and usually some time later, when the pressure profile becomes too peaked, these discharges disrupt with coupling to a global mode.[22] A developing instability for these modes might explain why ∇T_e becomes small near the axis and the ETG modes become stable. However, it should be noted that similar GKS analysis during the low power phase for this shot (t = 1.52 s) showed the ETG modes stable and $D_R < 0$, indicating some other turbulence process(es) may have a role near the axis.

Many DIII–D discharges with an internal ITB and L–mode edge show progressive flattening of profiles near the axis and a correlation of *decreasing* a/LT_e with *increasing* Shafranov shift, defined by the normalized pressure gradient (ballooning parameter) $\alpha = -q^2 R_0 \nabla \beta_t$. Here R_0 is the mean major radius of the flux surface, and β_t is the local total toroidal beta. Figure 3 shows the correlation, near the

axis at $\rho = 0.2$, during the discharge evolution for four high power beam heated shots. Also shown at low and high α are the T_e, T_i, and n_e profiles which clearly show greater flattening near the axis with increased α.

We have not determined an explicit dependence of a/LT_e on parameters, but the trend is for less core flattening to occur for discharges with lower magnetic shear. The correlation may indicate some pressure gradient driven process producing turbulence and profile flattening. The smaller temperature gradient is manifest in larger thermal diffusivity near the axis, as inferred from transport analysis. A similar trend toward flatter profiles is also observed in the ion temperature and toroidal rotation profiles. The trend for the electron density is opposite, with peaking in the density profile, not flattening, at higher α.

D. Transport in strong negative magnetic shear

A clear electron transport barrier is demonstrated with strong negative magnetic shear (Fig. 4). The plasma was formed in the standard way by early beam injection, but with an initially faster current ramp up to 0.8 MA, followed by a slower ramp up to 1.6 MA. Plasma profiles at $t = 0.88$ s near the end of ramp up are shown in Fig. 4. MHD fluctuations were highly visible during much of the discharge, but the profiles shown in Fig. 4 are from a period with very low MHD activity. Large gradients in T_i and toroidal rotation Ω also occur in the same region as the large T_e gradient. Several important features of the profiles are: 1) the coincidence of the steep electron and ion temperature gradients, and 2) ∇T_e is very small inside $\rho = 0.3$. The T_i profile peaks on axis and the ω_{tor} profile becomes flat inside $\rho \approx 0.18$. The very flat T_e profile implies large electron diffusivity inside $\rho \approx 0.3$.

Results from transport analysis for the diffusivities and comparison with GKS calculations are plotted in Fig. 5 for ions and in Fig. 6 for electrons. Figure 5(a) shows the rapid decrease of χ_i^{tot} to the neoclassical level inside $\rho = 0.4$. Shown for reference is the profile for χ_e^{tot}. Both diffusivities decrease rapidly within the beginning ITB where $\omega_{ExB} > \gamma_{max}$, but then increase further inside toward the magnetic axis. The radial extent of strong depression is narrower for the electrons than the ions. The stability calculation for the low k ITG mode and the measured ExB flow shear profiles are compared in Fig. 5(b). Similar to the result for the low shear discharge, $\omega_{ExB} \geq \gamma_{max}$ inside the ITB for $\rho \leq 0.4$,

where∇T_i is large, again consistent with suppression of low k modes. For co-injected beams, the pressure gradient term in the carbon impurity force balance equation for E_r opposes the $\vec{v} \times \vec{B}$ term. This causes a rapid change in E_r where∇T_i is large, and the flow shear profile determined from $d/d\psi$ (E_r/RB_t) becomes very peaked at $\rho = 0.28$.

For the electrons, χ_e^{tot} decreases about a factor 3 to ~0.15 m^2-s^{-1} at $\rho = 0.35$. Because ∇T_e is large only over a narrow radial extent, the diffusivity increases to a much larger value inside $\rho = 0.25$, where the T_e profile is very flat. The magnitude of the minimum χ_e^{tot} is similar to that reported in JET[23] and JT60-U.[24] Similarly, χ_e increases near the axis in both machines. For JET, MHD is a suspect for the cause of the increase in χ_e toward the magnetic axis.

We compare the experimental gradients and ETG critical gradient for the electrons in Fig. 6(a) In the region of strong χ_e^{tot} reduction, the experimental and ETG critical gradients track together. As the critical gradient increases, the experimental gradient rises in response. Because $a/L_{T_e}^{\exp} > a/L_{T_e}^{crit}$ near the maximum value of $a/L_{T_e}^{\exp}$, the ETG mode is unstable. Figure 6(c) shows the GKS spectrum calculated at the peak experimental gradient ($\rho = 0.36$). The ETG mode is unstable for $20 < k <$ 100 cm^{-1}, where $\gamma > \omega_{ExB}$. These unstable modes could limit the rise of ∇T_e and, therefore, the reduction of χ_e^{tot}.

This strong magnetic shear result, in addition to the result with low magnetic shear, provides good support for the hypothesis that χ_e and thus ∇T_e is limited by ETG modes within a narrow region just inside of an ITB. At smaller radius again the T_e profile flattens, and the ETG mode is stable, suggesting, once again, that some other process controls electron transport.

The normalized pressure gradient, α, and magnetic shear, S, profiles for low and stronc NCS plasmas are compared in Fig. 7(a). Where the ETG mode appears to control transport in both plasmas (heavy lines in the figure), s was small or positive in the weak magnetic shear discharge, and ∇T_e was relatively small. For the strong negative shear plasma, ∇T_e was large where magnetic shear was *strongly negative*. The Shafranov shift (α) values were similar. The q profiles and normalized electron density gradients for the two discharges are shown in Fig. 7(b). Here the safety factor values were similar, but density peaking was *larger* in the discharge with weak negative shear.

From the GKS theory, large α, large negative magnetic shear s, and density peaking are important stabilizing terms for the ETG modes. Comparing the two discharges (heavy lines), experimentally It appears that large and negative s was the more important quantity for large∇T_e and reduced electron transport for DIII–D. This agrees with experience in other machines where large and negative s is recognized as a key parameter for obtaining an electron ITB in other machines.[8]

III. FLUCTUATION MEASUREMENTS AND AUXILIARY HEATING

Within the context of our transport studies in NCS discharges, in order to better understand the anomalous electron transport, we have employed auxiliary electron heating (EH), using both fast wave (FW) and electron cyclotron heating (ECH) power.[24] The experiments were motivated by observations that heating of core electrons within an ITB degraded the ITB and increased thermal diffusivities. These effects were independent of the electron heating method, with similar results for both FW[25] and ECH. Because the heat deposition profile of ECH is known more accurately and is more controllable than fast waves, ECH was used for the results reported here. Because the effects on transport were reproducible, EH provided a powerful tool to both change and diagnose transport behavior. During these experiments, we used FIR forward scattering to measure short wavelength fluctuations at $k = 6$, 9, and 12 cm^{-1}.

The general behavior of plasma parameters, in a plasma with beam heating only are compared to those of a similar discharge with EH added (1.1 MW) in Fig. 8. Figure 8(a) shows the timing sequence for heating sources, with an overlap period for EH and beam heating. Central temperatures T_{e0} and T_{i0} are also compared for the time with beam heating only and EH added in Fig. 8(b). With application of the EH, T_{e0} doubles, but T_{i0} decreases until the increase in beam heating increases T_i. The power balance transport results from TRANSP, plotted in Fig. 8(b,c) show diffusivity increases for both species with EH. The large increase of central χ_e is consistent with the modesl increase in T_e with the direct EH, a much smaller increase than expecteds if χ_e remained unchanged.

Figure 8(d-f) show the changes with EH in profiles for T_i, T_e, and carbon impurity toroidal rotation Ω at $t = 1.45$. It is clear that central deposition of the EH affected a large volume of the plasma, reduced central T_i and Ω 20%–40%, and caused shrinkage of the ITB. Thermal diffusivity profiles for ions and electrons (Fig. 9) reveal the smaller radius of the ITB and the large increase in χ_e with EH.

In these plasmas we have obtained FIR scattering measurements of high k fluctuations within a wavelength range which might strongly affect electron transport. These measurements are difficult to make, and our data set is preliminary and limited. With EH we have measured increased fluctuations at $k = 12$ cm^{-1} near the axis at $\rho = 0.1$. Unfortunately, we have no measurements at the same location

without EH, so we show a measurement at $\rho = 0.3$ for comparison. At this location fluctuations did not increase above the noise level of the diagnostic with EH. These results are shown in Fig. 10. These fluctuations rotate in the electron diamagnetic drift direction, consistent with the ETG mode. In this same location there was no evidence of an increase with EH of fluctuations at $k = 6$ and 9 cm^{-1}.

Comparing the two discharges, a general summary of the results from these experiments is the following: the GKS calculations predict *no unstable* modes at *any k* inside $\rho = 0.3$, with or without EH. The EH affects both electron and ion transport and toroidal rotation as shown, in a way not yet understood. But, the transport behavior for the ions inside and outside the ITB agrees with the hypothesis of *ExB* flow shear suppression of ITG turbulence, for the measured *ExB* flow shear, which changes with EH.

High k fluctuations measured near the axis offer a clue pointing to some process, perhaps not ETG modes, that could increase electron transport, and perhaps ion transport as well, in some unexplained way. Microtearing modes are one possibility under investigation. It should be noted that in these experiments, Z_{eff} was unusually high for DIII–D [$Z_{eff}(0)$~3.8, compared to ~1.5 typical for most of our other NCS discharges]. The measured high *carbon* density stabilized the ETG mode near the axis according to the GKS calculations. For *all* the transport experiments reported in this paper, electron transport near the axis is not explained by the drift ballooning mode theory included in the GKS theory.

IV. Discussions and Summary

Comparison of GKS predictions with experiments in DIII–D, in low and strongly negative magnetic shear plasmas with an ITB, provide improved understanding for ion and electron thermal transport within much of the plasma. As previously reported, the region for improved ion transport seems well characterized by the condition $\omega_{ExB} > \gamma_{max}$, where ω_{ExB} is the *ExB* flow shear rate, calculated from measured quantities, and γ_{max} is the maximum calculated linear growth rate for ITG modes in the absence of flow shear. For the electrons, within a limited region just inside the point of ITG mode suppression, the ETG modes appear to dominate the electron thermal transport and, consequently, to provide a lower limit on electron thermal diffusivity

Our understanding of transport near the magnetic axis is incomplete. Calculations of ETG mode stability, using linear drift ballooning mode theory, does not explain the observed transport *near the axis*, and there are likely one or more other processes which must control transport in this region. Fluctuation measurements show the presence of high k turbulence which could impact electron transport and possibly also ion transport. Processes under consideration include resistive interchange and micro tearing.

Acknowledgments

This is work was supported by the U.S. Department of Energy under Contract Nos. DE-AC03-89ER51114 and W-7405-ENG-48, and Grant Nos. DE-FG03-86ER53225, DE-FG03-97ER54415, and DE-FG02-92ER54139 at Lawrence Livermore National Laboratory.

References

[1]C.M. Greenfield, D.P. Schissel, B.W. Stallard, E.A. Lazuras, G.A. Navratil, K.H. Burrell, T.A. Casper, J.C. DeBoo, R.J. Fonck, C.B. Forest, P. Gohil, R.J. Groebner, M. Jakubowski, L.L. Lao, M. Murakami, C.C. Petty, C.L. Rettig, T.L. Rhodes, B.W. Rice, H.E. St. John, G.M. Staebler, E.J. Strait, T.S. Taylor, A.D. Turnbull, K.L. Tritz, R.E. Waltz, and the DIII-D Team, Phys. Plasmas **4**, 1596 (1997).

[2]M.G. Bell, S. Batha, M. Beer, et al., Phys. Plasmas **4**, 1714 (1997).

[3]S. Ishida and The JT-60 Team, in *Plasma Physics and Controlled Nuclear Fusion Research* Proc. 17th International Conf., Yokohama, 1998 (International Atomic Energy Agency), Paper CN-69/OV1/1, to be published.

[4]M.L. Watkins and The JET Team, in *Plasma Physics and Controlled Nuclear Fusion Research* Proc. 17th International Conf., Yokohama, 1998 (International Atomic Energy Agency), Paper CN-69/OV1/2, to be published.

[5]T.S. Hahm and K.H. Burrell, Phys. Plasmas **2**, 1648 (1995).

[6]R.E. Waltz, G.D. Kerbel, J. Milovich, and G.W. Hammett, Phys. Plasmas **2**, 2408 (1995); ibid **1**, 2229 (1994); ibid **5**, 1784 (1998).

[7]C.L. Rettig, K.H. Burrell, B.W. Stallard, G.R. Mckee, G.M. Staebler, T.L. Rhodes, C.M. Greenfield, and W.A. Peebles, Phys. Plasmas **5**, 1727 (1998).

[8]H. Shirai, M. Kikuchi, T. Yakizuka, T. Fujita, Y. Koide, G. Rewolt, D. Mikkelsen, R. Budny, W.M. Tang, Y. Kishimoto, Y. Kamada, T. Oikawa, O. Naito, T. Fukuda, N. Isei, Y. Kawano, M. Azumi, and the JT-60 Team, in *Plasma Physics and Controlled Nuclear Fusion Research* , Proc. 17th International Conf., Yokohama, 1998 (International Atomic Energy Agency), Paper CN-69/EX5/4.

[9]V.V. Parail and the JET Team, in *Plasma Physics and Controlled Nuclear Fusion Research* Proc. 17th International Conf., Yokohama, 1998 (International Atomic Energy Agency), Paper F1-CN-69/ EX 6/1, to be published.

[10]R.E. Waltz, G.M. Staebler, W. Dorland, G.W. Hammett, M Kotchenreuther, and J.A. Konigs, Phys. Plasmas **4**, 2482 (1997).

[11]W. Horton, B.G. Hong, and W.M. Tang, Phys. Fluids **31**, 2971 (1988).

[12]R.J. Hawryluk, in Proc. of the Course in Physics Close to Thermonuclear Conditions, Varenna, 1979 (Commision of the European Communities, Brussels, 1980).

[13]P. Gohil, et al., in Fusion Technology (Proc. 14th Symp. San Diego, 1991), 2, IEEE, Princeton, NY (1992) 1199.

[14]L.L. Lao, et al., Phys. Fluids **28**, 869 (1985).

[15]B.W. Rice, K.H. Burrell, L.L. Lao, Nucl. Fusion **37**, 517 (1997).

[16]M. Kotschenreuther, G. Rewoldt, and W.M. Tang, Comp. Phys. Comm **88**, 128 (1995).

[17]R.E. Waltz and R. L. Miller, Bull. Am. Phys. Soc. **43,** 2001 (1998).

[18]R.L. Miller, M.S. Chu, J.M. Greene, Y.R. Lin-Liu, and R.E. Waltz, Phys. Plasmas **5**, 973 (1998).

[19]R.L. Miller, private communication.

[20]A.H. Glasser, J.M. Greene, and J.L. Johnson, Phys. Fluids **18**, 875 (1975); J.M. Greene, Comments Plasma Phys. Controlled Fusion, **17**, 389 (1997).

[21]M.S. Chu, J.M. Greene, L.L. Lao, R.L. Miller, A. Bondesson, O. Sauter, B.W. rice, E.J. Strait, T.S. Taylor, and A.D. Turnbull, Phys. Rev. Lett. **77**, 2710 (1996).

[22]X. Litaudon, T. Aniel, Y. Baranov, D. Bartlett, A. Becoulet, C. Challis, G.A. Cotrell, A. Ekedahl, M. Erba, L. Eriksson, C. Gormezano, G.T. Hoang, G. Huysmans, F. Imbeaux, E. joffrin, M. Mantsinen, V. parail, Y. Peysson, F. Rochard, P. Schild, A. Sips, F.X. Soldner, B. Tubbing, I. Voitsekhovitch, D. Ward, and W. Zwingmann, in *Proc. of the 25th European Conf. on Controlled Fusion and Plasmas Physics* (European Physical Society, Prague, Czech Republic, 1998), Part II, paper To.51, to be published.

[23]T. Fujita, et al., Phys. Rev. Lett. **78**, 2377 (1997).

[24]C.M. Greenfield, G.M. Staebler, K.H. Burrell, J.C. DeBoo, J.S. deGrassie, P.Gohil, C.C. Pety, R.I. Pinsker, R.E. Waltz, C.L. Rettig, E.J. Doyle, W.A. Peebles, T.l. Rhodes, L. Zeng, B.W. Stallard, B.W. Rice, M.E. Austin, G.R. McKee, and E.J. Synakowski, in *Plasma Physics and Controlled Nuclear Fusion Research*, Proc. 17th. International Conf., Yokohama, 1998 (International Atomic Energy Agency), Paper F1-CN-69/Ex5/5.

[25]G.M. Staebler, R.E. Waltz, C.M. Greenfield, B.W. Stallard, M.E. Austin, K.H. Burrell, J.S. deGrassie, E.J. Doyle, R.J. Groebner, G.L. Jackson, M. Kotchenreuther, L.L. Lao, Y.R. Lin-Liu, T.C. Luce, M. Murakami, C.C. Petty, R.I. Pinsker, P.A. Politzer, R. Preter, C.L. Rettig, T.L. Rhodes, B.W. Rice, R.D. Stambaugh, H.E St. John, and W.P. West, Proc. 1998 ICPP and in *Proc. of the 25th European Conf. on Controlled Fusion and Plasmas Physics* (European Physical Society, Prague, Czech Republic, 1998), Part II, paper P3.192, to be published.

List of Figure Captions

Fig. 1. Profiles for low magnetic shear discharge: (a) T_e, T_i, and the safety factor and (b) electron and ion thermal diffusivities. Profiles are shown at low power (t = 1.52 s) and high power (t = 1.82 s).

Fig. 2. GKS predictions for ITG and ETG mode stability: (a) γ_{max} for the ITG mode and the ω_{ExB} flow shear rate (shaded region is ITG stable) and (b) profiles of a/L_{T_e} for the experiment and for the ETG mode critical gradient at t = 1.82 s (U = unstable region).

Fig. 3. (a) Correlation of a/L_{T_e} with α during discharge evolution for four discharges and representative T_e, T_i, and n_e profiles at (b) low α and (c) high α.

Fig. 4. Gradient steepening in a discharge with strong negative magnetic shear: (a) beam injection into fast initial current ramp up to create strong shear and profiles of (b) T_e and q, (c) T_i and n_e, and (d) Ω at t = 0.88 s.

Fig. 5. Ion stability in strong negative magnetic shear: (a) ion and electron diffusivity profiles, showing ITB, and q profile and (b) comparison of ω_{ExB} flow shear rate and predicted γ_{max} for the ITG mode.

Fig. 6. Electron ITB and GKS predictions of ETG mode stability in strong magnetic shear:. (a) comparison of a/L_{T_e} for the experiment and ETG mode critical gradient, showing an increase of a/L_{T_e} as $a/L_{T_e}^{crit}$ increases within the electron ITB, (b) electron diffusivity within the electron ITB, and (c) the linear growth rate spectrum γ as a function of poloidal wave number at ρ = 0.36, showing ITG and ETG mode regions and unstable ETG region where $\omega_{ExB} > \gamma$.

Fig. 7. Variables affecting ETG mode stability, comparing low (dashed) and strong (solid) magnetic shear discharges: (a) α and s and (b) q and a/L_{n_e}; the heavy shaded lines indicate regions where a/L_{T_e} responds to changes in $a/L_{T_e}^{crit}$.

Fig. 8. Effects of additional core electron heating within a beam heated discharge: traces of (a) P_{ECH}, P_{NBI}, $T_i(0)$, and $T_e(0)$, (b) ion and (c) electron diffusivities; profiles of (d) T_i, (e) T_e, and (f) Ω.

Fig. 9. (a) ion and (b) electron diffusivity profiles compared with and without additional EH at t = 1.45 s (vertical line in Fig. 8).

Fig. 10. Fluctuations at 12 cm^{-1}, measured by FIR scattering, showing an increase at $\rho = 0.1$ with central EH, compared with measurement at $\rho = 0.3$ without EH; spatial resolution $\delta r \sim \pm 0.15$.

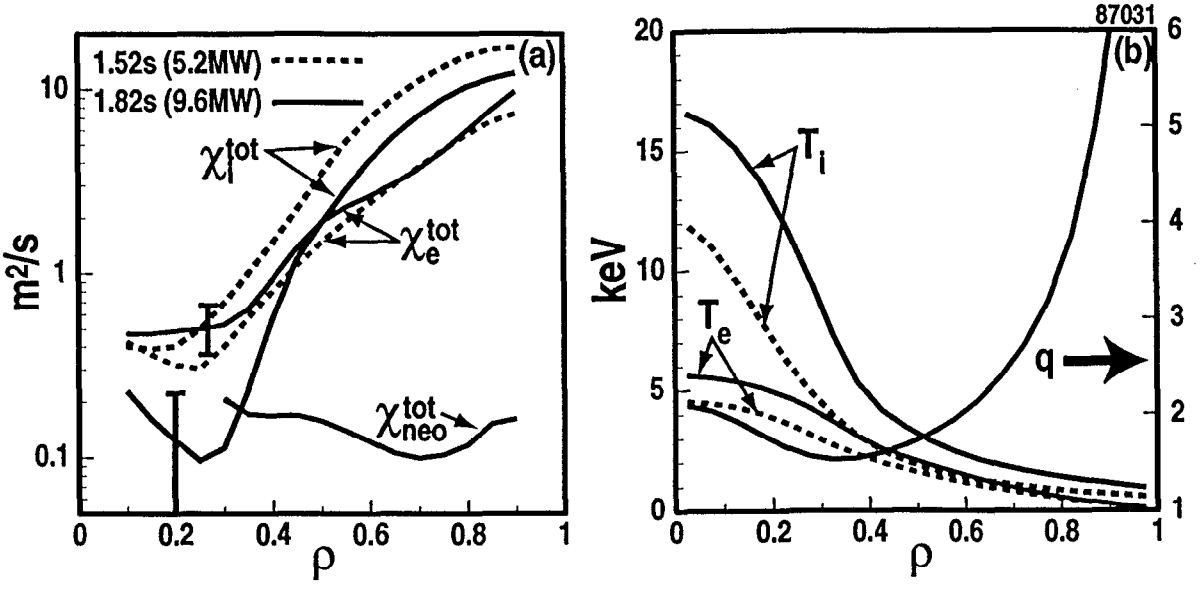

Stallard, B.W. Figure 1

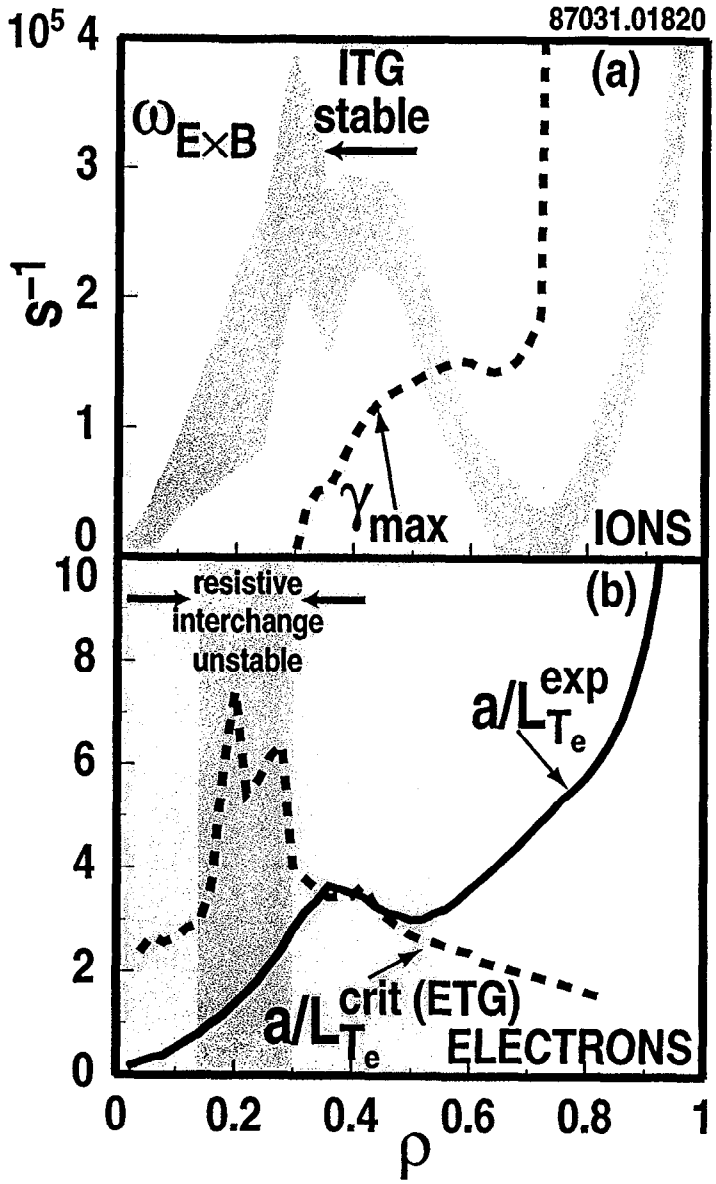

Stallard, B.W. Figure 2

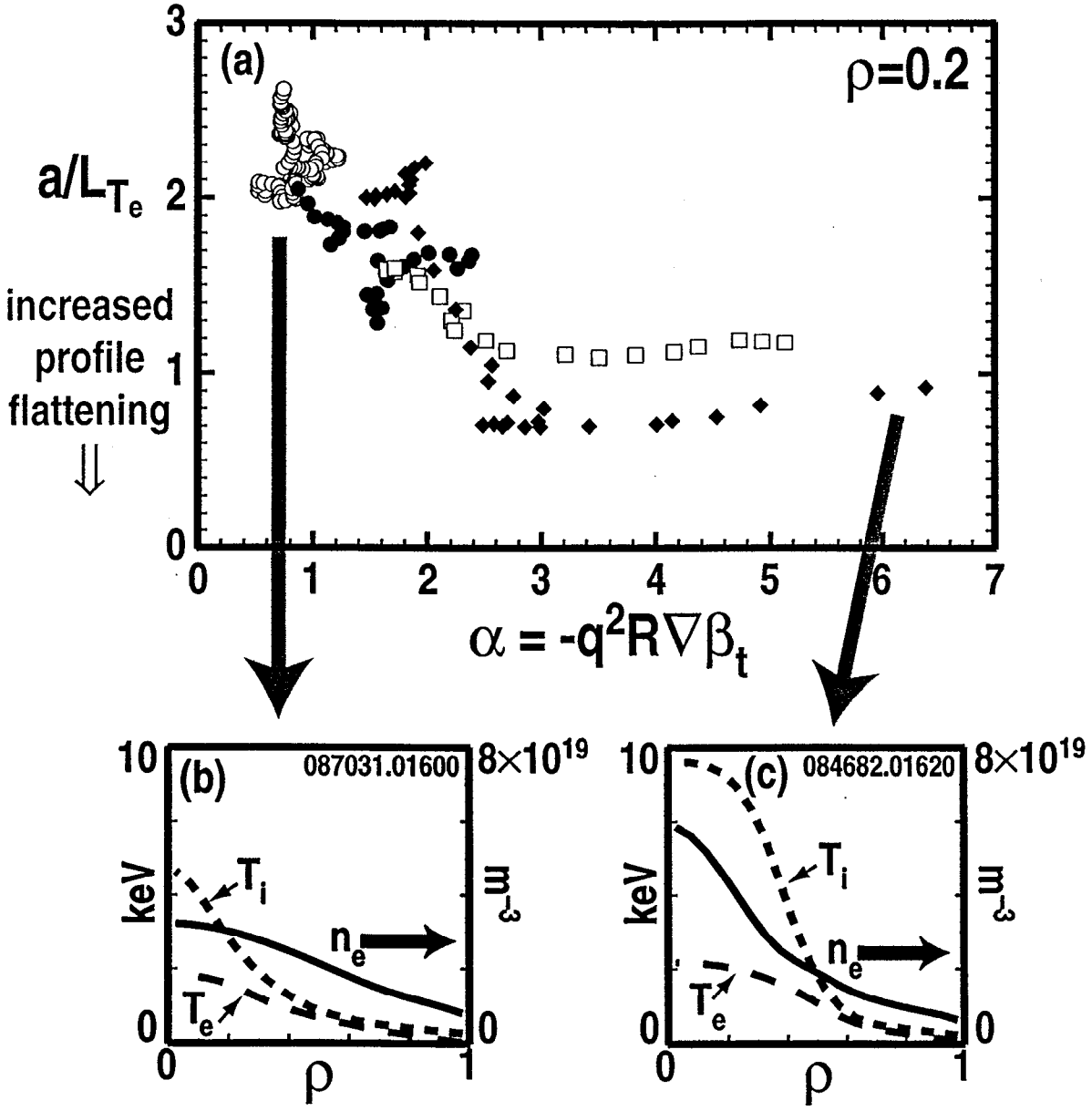

Stallard, B.W. Figure 3

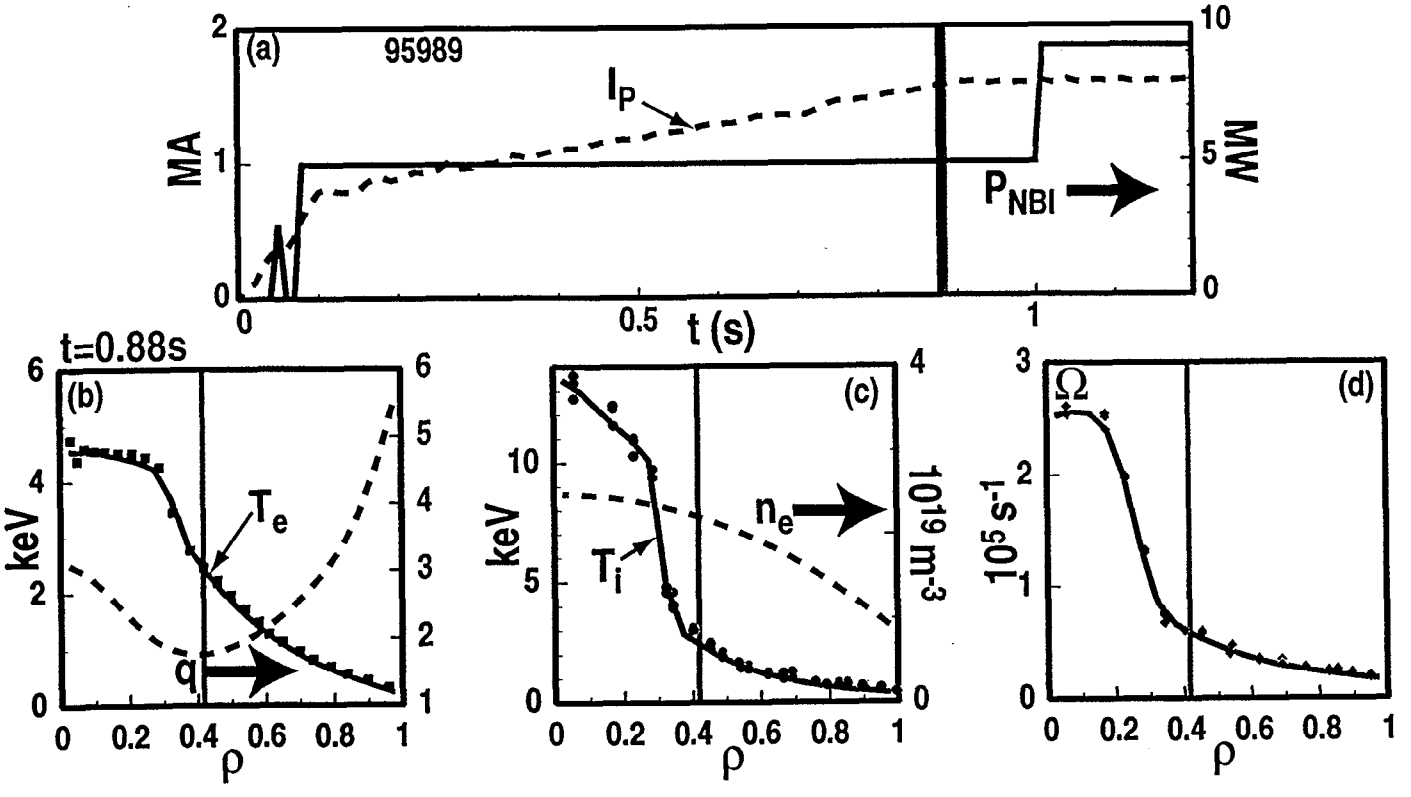

Stallard, B.W. Figure 4

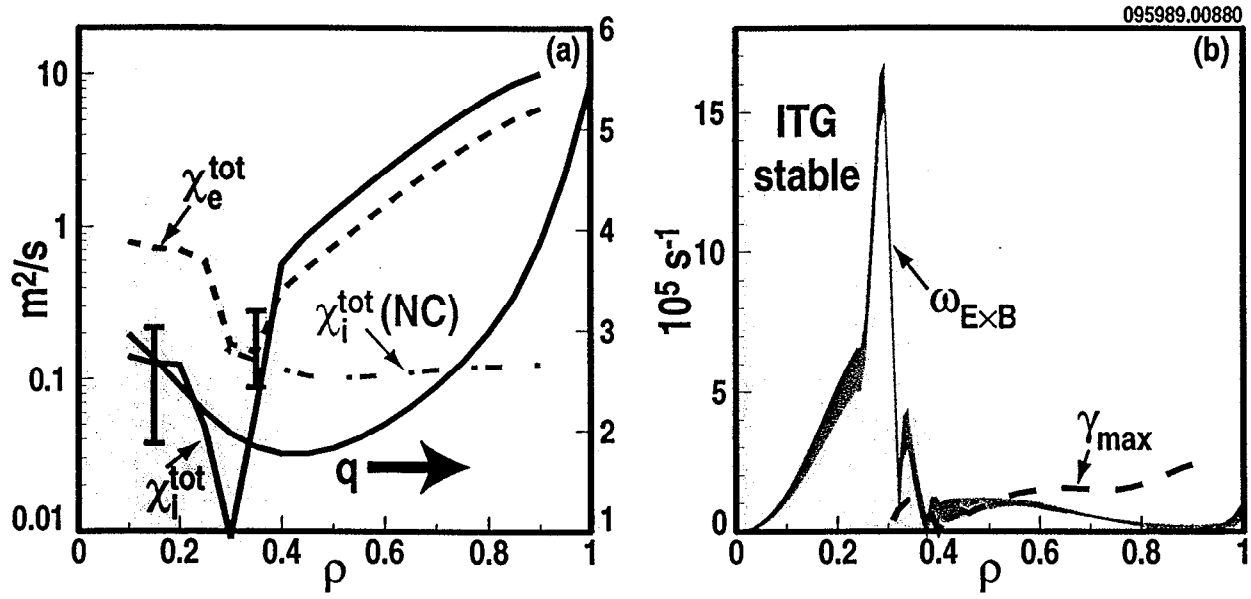

Stallard, B.W. Figure 5

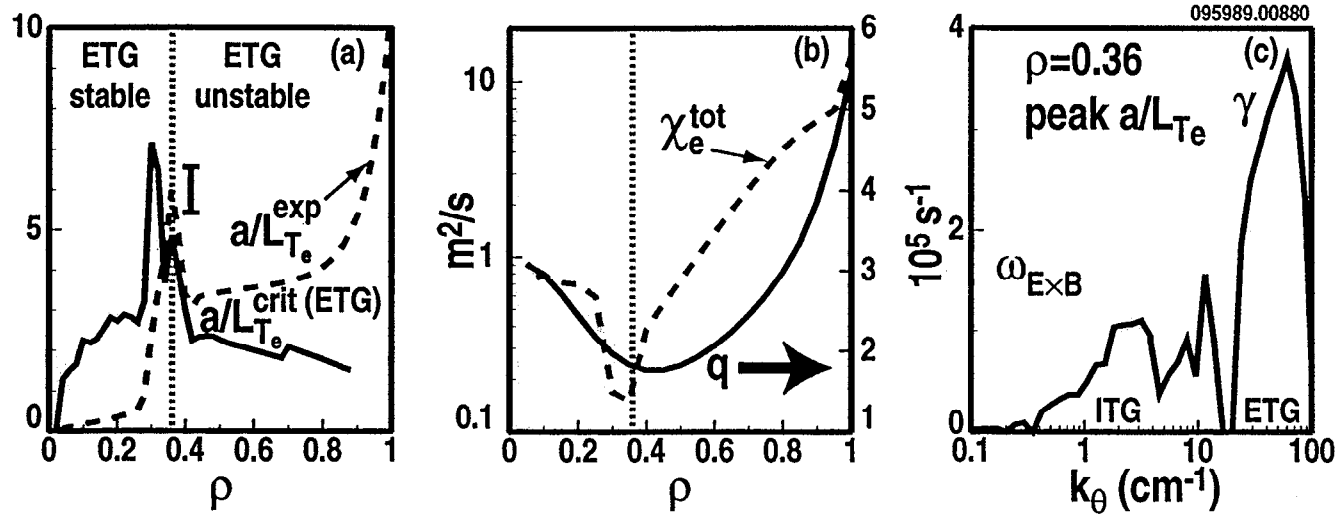

Stallard, B.W. Figure 6

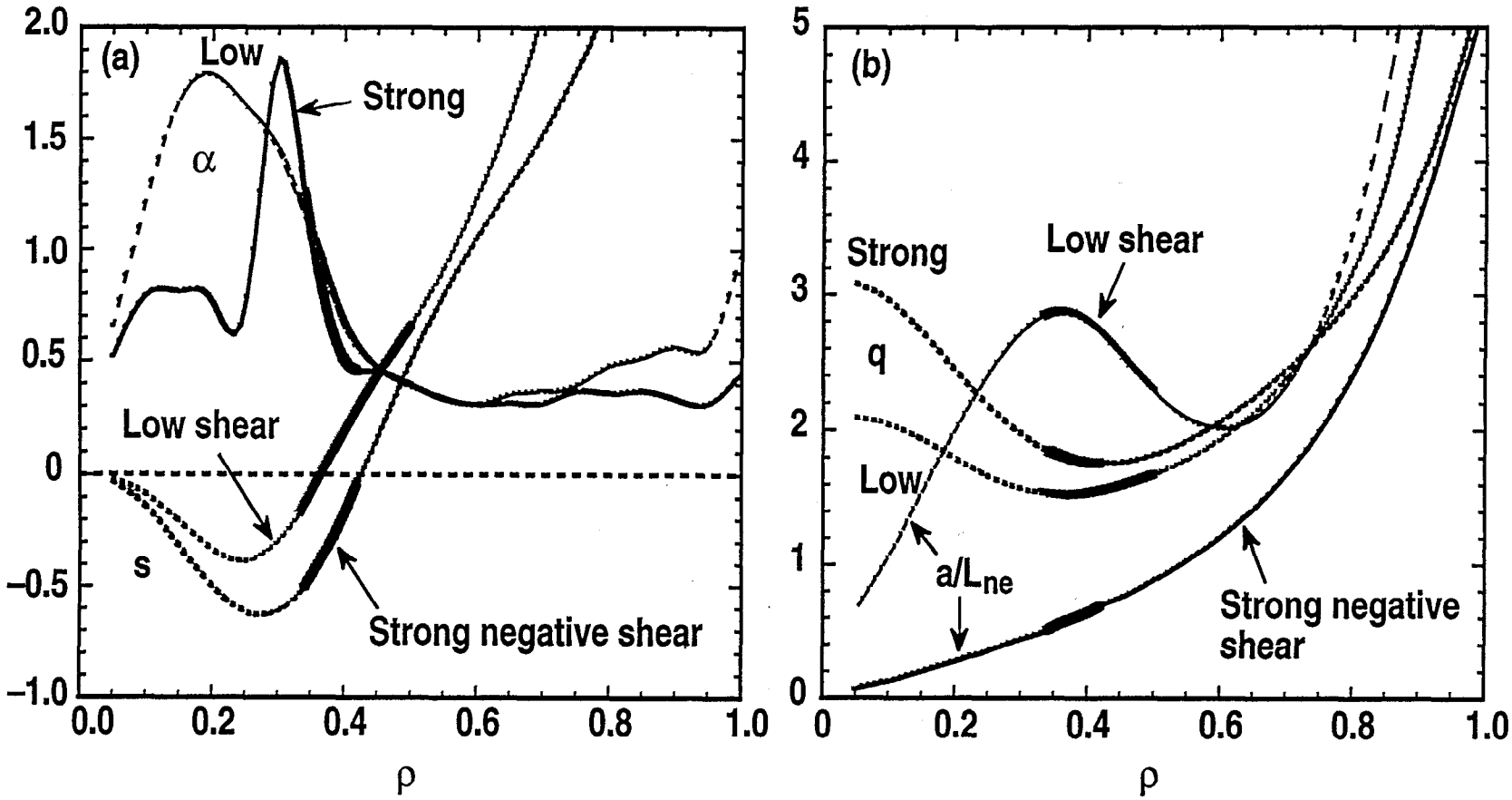

Stallard, B.W. Figure 7

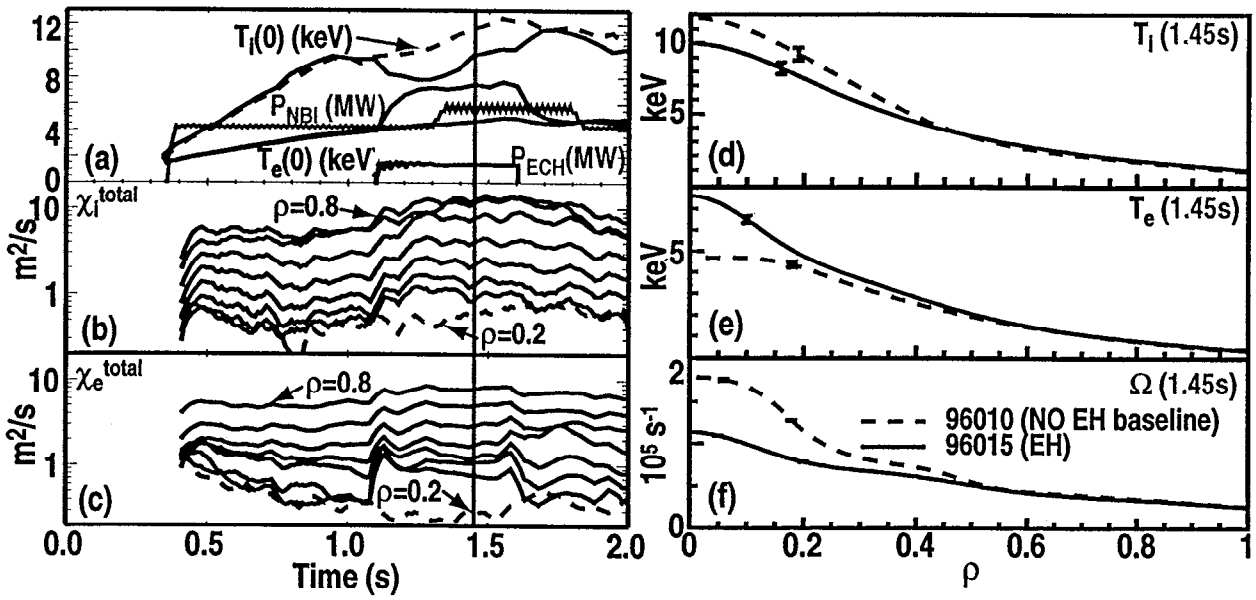

Stallard, B.W. Figure 8

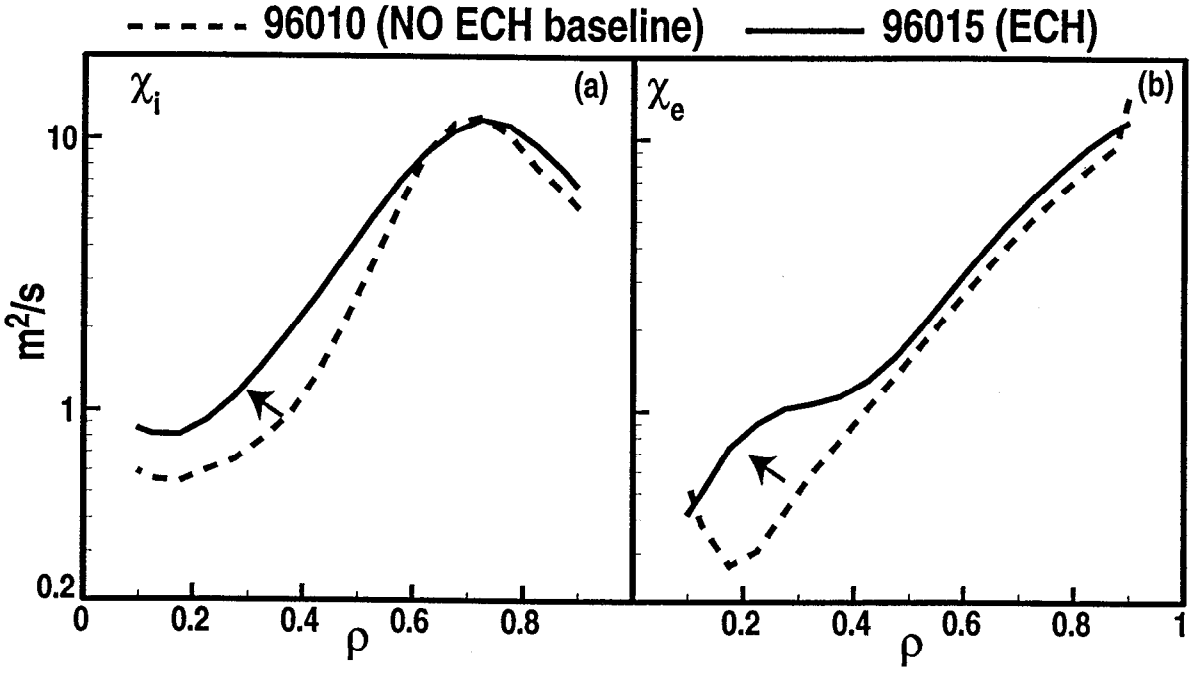

Stallard, B.W. Figure 9

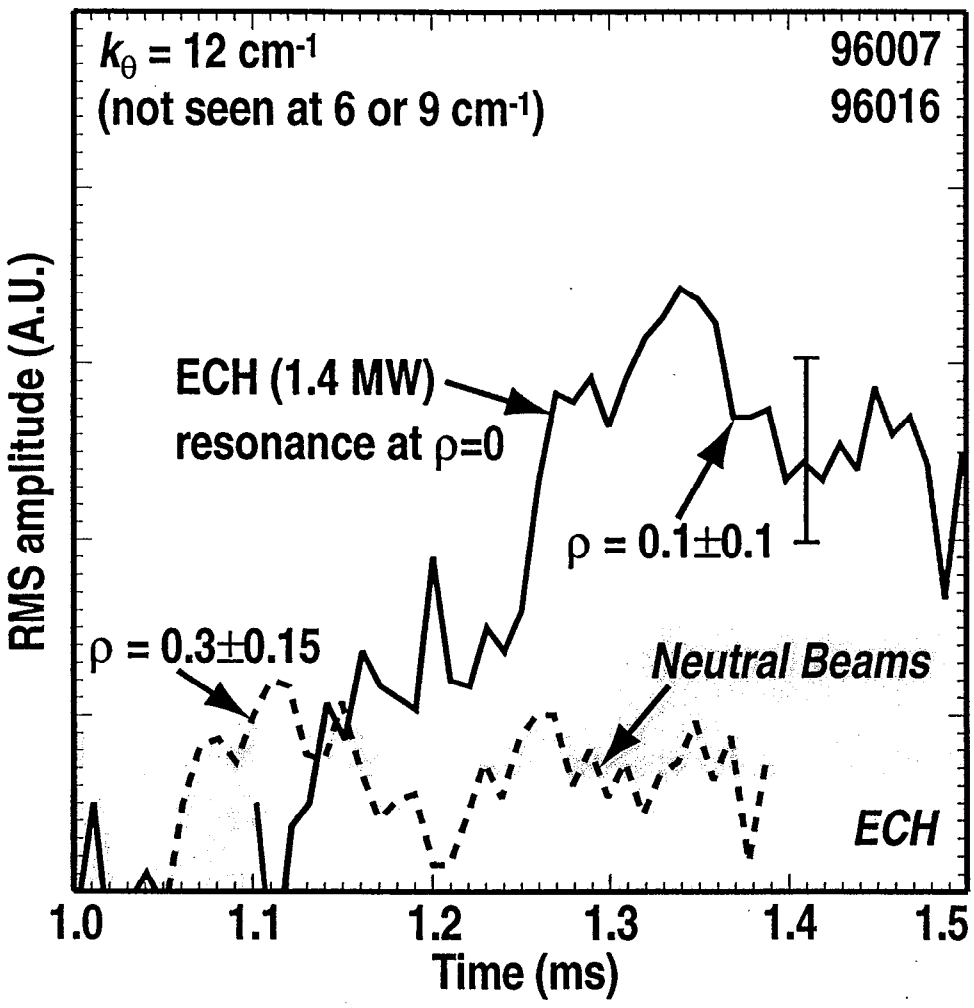

Stallard, B.W. Figure 10